UK Atomic Energy Authority

UKAEA-STEP-CP(23)03

James H.P. Rice, Jianzhao Geng, Rodney A. Badcock, Dominic A. Moseley, Steven Wray, Heng Zhang

Design of a Bifilar HTS Switching Element Using Iron-Core Field Coils

Design of a Bifilar HTS Switching Element Using Iron-Core Field Coils

James H.P. Rice, Jianzhao Geng, Rodney A. Badcock, Dominic A. Moseley, Steven Wray, Heng Zhang

This paper has been submitted to
27th International Conference on Magnet Technology, Fukuoka, Japan, 15-19 November 2021

Design of a Bifilar HTS Switching Element Using Iron-Core Field Coils

James H.P. Rice *Student Member, IEEE*, Jianzhao Geng, Rodney A. Badcock *Senior Member, IEEE*, Dominic A. Moseley, Steven Wray and Heng Zhang.

***Abstract*—The application of dc magnetic field to a 2G high temperature superconducting (HTS) tape can reduce the critical current I_c of the tape, without driving the material normal. This property can be used in the development of HTS switching elements through so-called $J_c(B)$ switching. The design of a dc magnetic field switch is reported, in both single and bifilar configurations. Dc magnetic field is applied by an iron-core field coil with copper windings, providing an applied field of up to 1.4 T. This allows for effective suppression of I_c. Here, it is also reported that the self-field I_c of the single tape is suppressed from 357 A to 195 A. This is due to the presence of the iron core amplifying and distorting the self-field of the tape and is confirmed by experiment and finite-element modelling. This effect can be eliminated using a bifilar configuration, which recovered close to the no-core self-field I_c of 357 A. Active dc switching by applied field was still achieved in the bifilar configuration. Such distortion and suppression may prove useful for the development of novel HTS circuit components.**

***Index Terms*—Flux pump, High-temperature superconductor, switch, transformer-rectifier**

I. Introduction

A COMMON application of High-Temperature Superconducting (HTS) materials is their use as a conductor in high-field magnets [1]. Low-inductance (<1 H) HTS magnets are seeing increased attention in areas where low-power, high-field magnets are advantageous, such as the toroidal field coils of magnetically-confined fusion energy [2]–[4] and space applications [5], [6]. Energizing such magnets to high magnetic fields requires large, dc currents; often in excess of 10 kA. Conventional current supplies capable of such outputs are bulky and expensive [7], making implementation of low-power, low-inductance magnets costly and difficult.

Alternatively, HTS flux pumps are superconducting dc power supplies [8], which operate as low voltage, high current power supplies [9]. They are capable of energizing superconducting magnets to currents >1 kA [10]–[12], and can maintain the output at large constant currents [13] with minimal loss [14]. Such output current is generated wirelessly within the cryostat [15], with such intra-cryogenic operation reducing cryogenic heat load by eliminating the need for current leads [16]. Overall, these characteristics make flux pumps an attractive choice for powering low-inductance magnets.

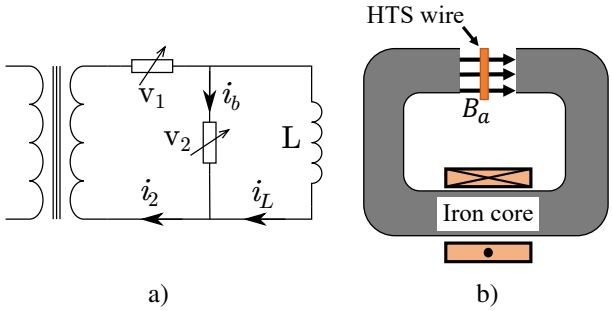

Fig. 1. a) Half-bridge topology of transformer-rectifier flux pump. Series and parallel HTS switching elements, v_1 and v_2, are shown as variable resistors, the load inductor L, and the transformer is taken to have a resistive primary and superconducting secondary connected to the load and parallel bridge components. b) Diagram of the electromagnet and applied field of the HTS switch. Current in the copper winding generates perpendicular applied field B_a for active control of the critical current of the HTS wire.

Flux pump topologies can based either on the linear travelling wave [10], [17]–[21] or transformer-rectifier [11], [12], [22]–[27] concepts. Transformer-rectifiers are of special interest due to their separation of the current generation and rectification components of the device. The circuit of a half-wave transformer-rectifier flux pump is illustrated in Fig. 1a). Ac current is generated in a superconducting circuit via transformer action, and is rectified into a dc voltage output by switching components [22]. The resistance of switching components can be generated by either dynamic resistance [9] or non-linear "flux creep" resistivity [23] and can be either passively [23] or actively [22] controlled. The load current is maintained between cycles by the bridge acting as a short for the load when voltage is not being generated. Switching components can be arranged in a half-bridge, full-bridge, or full-bridge center-tapped topology similar to conventional electronic rectifiers.

Recently, a transformer-rectifier flux pump with HTS switch elements utilizing only dc applied magnet field, so-called "$J_c(B)$ switching", has been reported [28]. In this device, the V-I relationship of the switching element is given by the non-linear resistivity of the superconducting switch element and the E-J power law [29]

$$V(I_t) = E_0 l \left(\frac{I_t}{I_c(B_a, T_{op})} \right)^n \tag{1}$$

This work was supported in part by the New Zealand Ministry of Business, Innovation and Employment (MBIE RTVU1916), and has been part-funded by STEP, a UKAEA programme to design and build a prototype fusion energy plant and a path to commercial fusion.

J.H.P. Rice, J. Geng, D.A. Moseley and R.A. Badcock are with the Robinson Research Institute, Victoria University of Wellington, Lower Hutt 5010, New Zealand. (e-mail: james.rice@vuw.ac.nz).

J. Geng is also with the Huazhong University of Science and Technology, Wuhan, Hubei, China.

S. Wray and H. Zhang are with the UK Atomic Energy Authority, Culham Science Centre, Abingdon OX14 3DB United Kingdom.

Manuscript received November 17th, 2021.

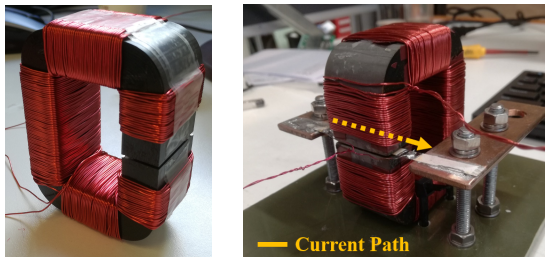

a) b)

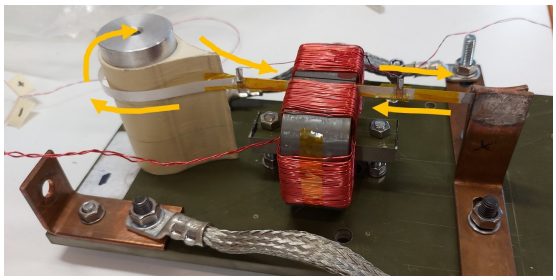

c)

Fig. 2. a) calibrated, iron-core electromagnet ($N = 405$ turns of ⌀0.6 mm enameled copper wire); b) the unifilar HTS switch test bed, where transport current is passed through the air-gap of the electromagnet in a); c) the bifilar HTS switch test bed, where transport current returns through the air-gap of the electromagnet in an anti-parallel fashion. Current paths for the unifilar and bifilar test beds are depicted in yellow.

where $E_0 = 1.0$ μV/cm is the conventional critical current criterion, l is the length of HTS wire in the switching element, I_t is the transport current, $I_c(B_a, T_{op})$ is the critical current at a given applied field B_a and operational temperature T_{op}, and n is the n-value of the exponential transition between the superconducting and normal states. By varying the applied field B_a, current in the bridge is driven above critical current in one part of the input ac current waveform only. This is similar to so-called self-rectifying flux pumps [11], [12], [23], [26], [27], [30], except switching is actively controlled. This leads to a time-averaged dc voltage across the load and dc current generation [20].

In this study, specific attention is given to the HTS switching element as a circuit component. A diagram of the switch geometry is shown in Fig. 1b), with experimental implementations depicted later in Fig. 2. Applied field is generated using an electromagnet with a core of high permeability material, with a switching element of HTS wire placed in the air-gap. This geometry applies magnetic field perpendicularly to the tape face. This type of topology has been used previously in dynamic-resistance switched transformer-rectifiers [22], [24], [25], as well as the recently reported $J_c(B)$-rectifier [28]. Following (1), the voltage can be increased by increasing the length of the switching element.As such, the HTS switch element may also be of a circular geometry for increased length [31]. There are still a number of unknowns relating to the behaviour of the HTS switching element as a circuit component, namely its critical current, circuit inductance, screening of applied field, and the use of HTS cables as switching elements. Here, we focus attention on the critical current behaviour of the HTS switch element, as it may directly limit the output current of the transformer-rectifier [12].

The paper is arranged as follows. The experimental method of critical current testing of a HTS switch element is described in Sec. II. This will include a descriptions of the critical current measurement system and the switching elements tested. Sec. III will present results of critical current measurements and compare results from switch elements to a reference of HTS wire performance. In Sec. IV, a finite-element vector-field model of the switch will be presented, and conclusions drawn on the critical current behaviour. Finally, the results will be summarized in Sec. V.

II. Experimental Method

An 'ex situ' test bed was produced to test the critical current behaviour of the HTS switching element outside of the flux pump. This test bed features a calibrated, iron-core electromagnet for applying a homogeneous, perpendicular magnetic field to the HTS wire sample. The test bed was secured to a G10 board and submerged in liquid nitrogen (LN2). The critical current of the sample was then tested using a 4-wire measurement system. For reasons that will become clear later, two test beds were fabricated; both using the same calibrated electromagnet, which is seen in Fig. 2a) and detailed in Sec. II-B. One test bed employed the single-tape switching element seen in Fig. 2b), hereafter referred to as the unifilar configuration. The other test bed includes an anti-parallel return path for the switching element to minimize self-inductance, hereafter referred to as the bifilar configuration shown, in Fig. 2c).

A. Critical Current Measurements

Transport current was supplied by an Agilent 6681a dc current supply, capable of supplying up to 580 A of current through the switching element sample. Voltage taps were soldered to the sample 35 mm apart, and the voltage across the sample was measured with using an Agilent 34420a nanovolt meter (NVM). The resulting voltage was divided by the sample length under applied field, or distance between voltage taps in the case of zero field, to obtain the electric field in μV/cm. Transport current in the sample was increased in a step-wise fashion, with measurements of voltage at each voltage step to build a V-I response of the tape. Steps of 5 A were used up to 90% of I_c, then steps of 0.1 A until a suitable voltage threshold of 0.8-1.0 μV/cm was reached. The current was then decreased in the reverse fashion, offset by 0.1 A to ensured measurements did not suffer from hysteresis. V-I responses were analyzed against the 1.0 μV/cm critical current criterion. Data points below the level of detectable noise (typically 0.05 μV/cm for 30 mm samples) were excluded from the analysis. Analysis was performed using linear fitting of the log-log dependence of the voltage on transport current [32]. Taking the logarithm of (1),

$$\ln\left(\frac{V(I_t)}{l}\right) = n\left[\ln\left(I_t\right) - \ln\left(I_c(B_a)\right)\right], \tag{2}$$

the critical current and n-value can be obtained from linear fitting of (2) as

$$I_c\left(B_a\right) = -\frac{c}{n} \tag{3}$$

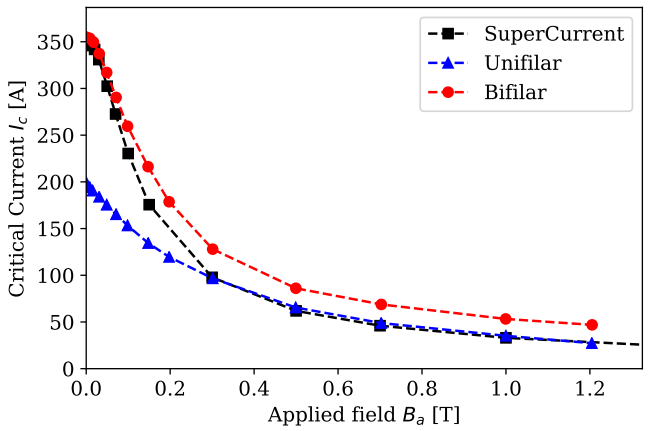

Fig. 3. Critical current response of SCN06300-210310-01 samples in the unifilar (blue) and bifilar (red) test beds under applied field up to 1.2 T. These are compared to critical current data provided by SuperCurrent [33], [34].

where c is the y-intercept of the linear fit, and n is the slope.

B. Calibrated Iron-core Electromagnet

The electromagnet was made from ⌀0.6 mm copper wire wound around a C-shaped iron core made of laminated 0.23 mm steel. The iron core had a rated saturation flux density of 1.9 T at room temperature, which was reduced to 1.35 T in LN2. The core had outer dimensions of $(80 \times 60 \times 30)$ mm, an outer bend radius of 15 mm, and an inner bore of (50×30) mm. $N = 405$ turns of copper was used, and was measured using an LRC meter to have a room temperature series resistance of 3.06 Ω and an inductance of 93.6 mH. Field was applied to the sample in the 1 mm air-gap of the core, giving a switch element length of about 30 mm. Current was supplied to the coil by a Tenma 72-13330 bench-top dc power supply, capable of producing 5 A of coil current. The magnetic field in the air-gap of the coil was calibrated at 77 K in LN2 using a P15A hall sensor from Advanced Hall Sensors Ltd in the 1 mm air-gap. The field in the air gap was found to be linear to within 1% of 0.438 T/A up to about 1.1 T of applied field at 77 K.

III. Experimental Results

An HTS wire sample supplid by SuNAM Ltd. Co. (SCN06300-210310-01) was analyzed in both unifilar and bifilar configurations. The HTS wire was a 6 mm wide, 1.3 μm thick film of GdBCO ($T_c = 91$ K, $I_c = 357 \pm 5.5$ A @ 77 K) grown on a hastelloy substrate, anodized with a 2 μ layer of silver, and plated with 13 μm of copper. Results of critical current measurements of this wire as both a unifilar and bifilar HTS switch element as described in Sec. II are shown in Fig. 3.

The results shown in Fig. 3 are directly compared to commercial characterization of the same sample of HTS wire performed at the SuperCurrent facility at the Robinson Research Institute [33], [34]. This facility uses a 30 mm bore HTS magnet to apply field, and is treated as a control measurement of the $J_c(B)$ response of the sample. Notably, the unifilar switch element exhibits a 45% reduction in self-field critical current under no applied field. Critical current later converges with the database characterization beyond 0.3 T of applied field. This is somewhat larger than the penetration field $B_{p,\perp} = 4.9284\mu_0 I_c/\pi w$ =116 mT [35]. Upon repeating the experiment without the iron-core present, the database self-field I_c of 355 A was recovered. This indicates that the cause of the suppression of self-field Ic in this case is the presence of the iron-core of the electromagnet.

The bifilar switch element shows no such suppression of self-field I_c, instead showing a similar $J_c(B)$-response to the database characterization. At applied fields beyond about 0.1 T, the bifilar switch element shows less reduction in critical current due to applied field than the database characterization. This is roughly the penetration field of the wire, 116 mT, indicating this effect is caused by screening of applied field by the bifilar element, which acts as a stacked cable of two wires. Overall, the experimental results show the bifilar switching element has better $J_c(B)$-switching performance than the unifilar configuration based on its active modulation of critical current [14], [28].

IV. Vector-field Simulation

To investigate the cause of the critical current behaviour seen in Fig. 3, the switch coil geometry was replicated in COMSOL [36]. As the switch element is uniform along its length, the 2d geometry shown in Fig. 4 was studied. Dc magnetic field was applied by imposing a coil current of $I_{coil} \leq 2.3$ A produced a uniform 1.1 T in the air-gap of the iron-core. This matched the linear field response region of the calibrated electromagnet. The HTS wire was modelled as a 6 mm$\times$100 μm rectangle in the center of the 1 mm air-gap carrying uniform J_z whose total was equal to the transport current I_t. A bifilar model was also produced by adding a second HTS wire element, carrying an equal but negative transport current density in an identical cross section, vertically separated from the first element by 100 μm. The superconducting properties of the switch elements were not included, instead focusing on the magnetic field profile surrounding the HTS wire element. Modelled magnetic flux densities of both unifilar and bifilar configurations under self-field (B_a=0.0 T) and applied field (B_a=1.1 T) are shown in Fig. 5.

In the unifilar self-field case (Fig. 5a)), the applied field was 0.0 T and the switch carried 195 A of transport current to match the measured I_c of the switch. It is clear that the self-field of the switching element has been severely distorted by the iron-core, spreading the self-field linearly across the HTS wire. This is because one half of the self-field has taken the low-reluctance return path of the iron core. Moreover, the self-field without the iron-core was found to have a peak magnitude of about 70 mT at 355 A of transport current (not shown), but with the iron-core has been increased to about 300 mT at only 195 A of transport current. This is in agreement with the applied field at which the unifilar results converge with the database measurements. This distortion increases the magnetic field environment of the tape, causing the reduction in unifilar self-field seen in Fig. 3. In the unifilar applied field case

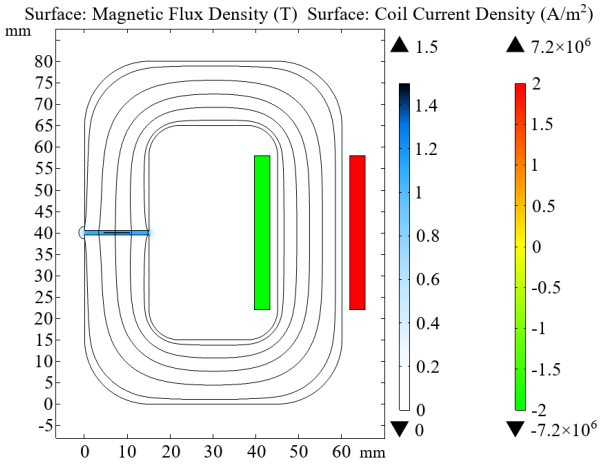

Fig. 4. Iron-core electromagnet geometry replicated in COMSOL Multiphysics. Central C-shaped core is modelled as a high permeability domain ($\mu_r = 4000$), and applied field is generated in the 1 mm air-gap on the left hand side by a pair of coil winding domains on the right hand side, shown in red and green. Coil current is applied by uniform current densities J_z of equal and opposite total current in the coil domains. The surrounding area is simulated as a region of vacuum permeability ($\mu_r = 1$). The superconductor domain is placed in the center of the air-gap, and transport current applied as uniform current density J_z with total current I_t.

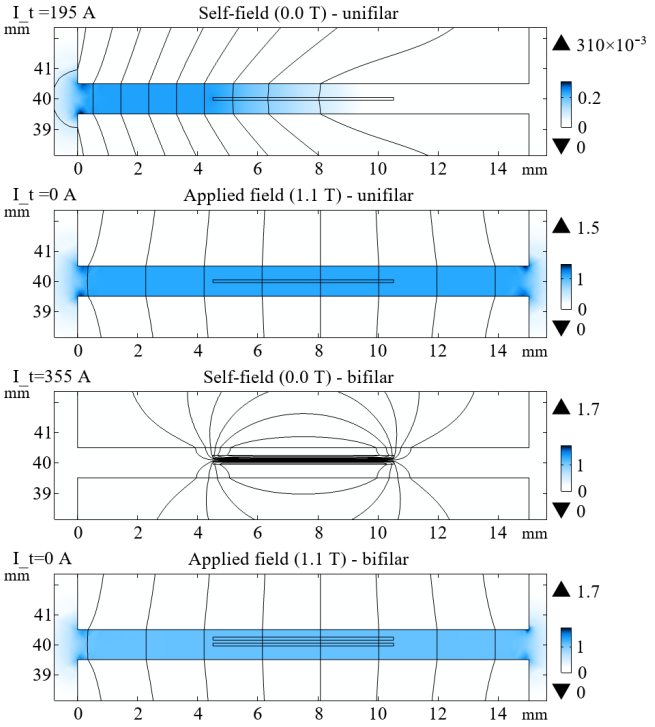

Fig. 5. Vector-field solutions for the model geometry shown in Fig. 4. Solutions presented are for a,c) the self-field (B_a=0.0 T) and b,d) applied field (B_a=1.1 T) cases, in both a-b) unifilar and c-d) bifilar configurations, displaying the region of interest in the air-gap. Solutions were performed using the built-in `mf` package with a stationary solver, and the magnitude of the magnetic induction (`mf.normH*mu0_const`) shown in blue, with contour lines of constant magnetic vector potential in black (`mf.Az`).

(Fig. 5b)), the applied field was increased to 1.1 T, and the transport current was set to 0 A. The field profile in the air-gap is dominated by the applied field of 1.1 T, causing the convergence of unifilar critical current with database results at increased applied field seen in Fig. 3.

The bifilar self-field case (Fig. 5c)) was simulated using an applied field of 0.0 T and 355 A of transport current. The bifilar configuration concentrated the self-field of the HTS switch element to be predominantly parallel to the tape faces between the two HTS wire elements. Additionally, the peak magnitude of the field was reduced to about 70 mT, similar to the case of a single HTS wire without the iron-core. These results show that interaction between the bifilar switching element and the iron-core is minimized in the bifilar case, preventing the suppression of self-field critical current seen in the unifilar case.

The bifilar applied field case (Fig. 5d)) had an applied field of 1.1 T and shows a homogeneous field profile in the air-gap, showing no screening of applied field in this case. This is because the model did not include the superconducting properties of the HTS wire. A more quantitative study could accurately include these properties by using T- or H-formulation [37]–[39] to numerically model the HTS tape domain. It is expected that including these properties would enable the model to replicate the behaviour of the bifilar element under applied field.

V. Conclusions

The critical current behaviour of a HTS switching element in the air-gap of a high permeability electromagnets was tested ex situ from the flux pump circuit. A test bed was produced which replicated the geometry of typically reported HTS switching elements in transformer-rectifier flux pumps. This employed a calibrated electromagnet with a C-shaped high-permeability iron core. Measurements of critical current of the HTS switching element in the air-gap of the iron core were performed, and results compared to database values of critical current obtained commercially. In the unifilar case, it was found that self-field critical current was suppressed by 45%, from 355 A to 195 A. This converged with database results for critical current under large applied fields >0.3 T. The suppression of critical current was prevented by the use of a so-called bifilar configuration, whereby the self-inductance of the HTS switching element was minimized by including a return path for the transport current through the air-gap. In the bifilar HTS switching element, the database self-field of 355 A was recovered. This provided better critical current modulation in the bifilar switching element than the unifilar case.

The cause of this suppression was investigated numerically using finite-element analysis. A 2d vector field model of the HTS switching element and the high-permeability electromagnet were produced. This revealed that in the unifilar case, the self-field of the HTS wire was increased and spread across the width of the tape, increasing the magnetic environment of the switch element and reducing its critical current. Interaction between the self-inductance of the HTS switch and the high-permeability core was minimized in the bifilar configuration, preventing suppression of critical current. This gave the bifilar HTS switch element better critical current behaviour for switching than the unifilar configuration.

References

[1] H. W. Weijers, U. P. Trociewitz, W. D. Markiewicz, *et al.*, "High field magnets with HTS conductors," *IEEE Transactions on Applied Superconductivity*, vol. 20, no. 3, pp. 576–582, Jun. 2010. DOI: 10.1109/TASC.2010.2043080.

[2] C. Sborchia, Y. Fu, R. Gallix, *et al.*, "Design and specifications of the ITER TF coils," *IEEE Transactions on Applied Superconductivity*, vol. 18, no. 2, pp. 463–466, Jun. 2008. DOI: 10.1109/TASC.2008.921339.

[3] A. Sykes, A. E. Costley, C. G. Windsor, *et al.*, "Compact fusion energy based on the spherical tokamak," *Nuclear Fusion*, vol. 58, no. 1, p. 016 039, Nov. 2017. DOI: 10.1088/1741-4326/aa8c8d.

[4] A. J. Creely, M. J. Greenwald, S. B. Ballinger, *et al.*, "Overview of the SPARC tokamak," *Journal of Plasma Physics*, vol. 86, no. 5, Oct. 2020. DOI: 10.1017/S0022377820001257.

[5] S. Schael, A. Atanasyan, J. Berdugo, *et al.*, "AMS-100: The next generation magnetic spectrometer in space - an international science platform for physics and astrophysics at lagrange point 2," *Nuclear Instruments and Methods in Physics Research Section A: Accelerators, Spectrometers, Detectors and Associated Equipment*, vol. 944, p. 162 561, Nov. 2019. DOI: 10.1016/j.nima.2019.162561.

[6] D. Chesny, G. Levin, L. Persons, *et al.*, "Galactic cosmic ray shielding using spherical field-reversed array of superconducting coils," *Journal of Spacecraft and Rockets*, vol. 57, pp. 1–10, May 18, 2020. DOI: 10.2514/1.A34710.

[7] Magna-Power, Flemington, New Jersey USA, "Datasheet: MT series high-power floor-standing programmable DC power supply,"

[8] T. A. Coombs, J. Geng, L. Fu, *et al.*, "An overview of flux pumps for HTS coils," *IEEE Transactions on Applied Superconductivity*, vol. 27, no. 4, pp. 1–6, Jun. 2017. DOI: 10.1109/TASC.2016.2645130.

[9] Z. Jiang, K. Hamilton, N. Amemiya, *et al.*, "Dynamic resistance of a high-Tc superconducting flux pump," *Applied Physics Letters*, vol. 105, no. 11, p. 112 601, Sep. 15, 2014. DOI: 10.1063/1.4895732.

[10] K. Hamilton, A. E. Pantoja, J. G. Storey, *et al.*, "Design and performance of a "squirrel-cage" dynamo-type HTS flux pump," *IEEE Transactions on Applied Superconductivity*, vol. 28, no. 4, pp. 1–5, Jun. 2018. DOI: 10.1109/TASC.2018.2805161.

[11] J. Geng, T. Painter, P. Long, *et al.*, "A kilo-ampere level HTS flux pump," *Superconductor Science and Technology*, vol. 32, no. 7, p. 074 004, Jul. 1, 2019. DOI: 10.1088/1361-6668/ab1821.

[12] J. Geng, C. W. Bumby, and R. A. Badcock, "Maximising the current output from a self-switching kA-class rectifier flux pump," *Superconductor Science and Technology*, vol. 33, no. 4, p. 045 005, Apr. 1, 2020. DOI: 10.1088/1361-6668/ab6957.

[13] S. Lee, W.-S. Kim, Y. Kim, *et al.*, "Persistent current mode operation of a 2g HTS coil with a flux pump," *IEEE Transactions on Applied Superconductivity*, vol. 26, no. 4, pp. 1–4, Jun. 2016. DOI: 10.1109/TASC.2016.2524519.

[14] J. H. P. Rice, J. Geng, C. W. Bumby, *et al.*, "Design of a 60 ka flux pump for fusion toroidal field coils," submitted manuscript, 2021.

[15] C. W. Bumby, A. E. Pantoja, H. Sung, *et al.*, "Through-wall excitation of a magnet coil by an external-rotor HTS flux pump," *IEEE Transactions on Applied Superconductivity*, vol. 26, no. 4, pp. 1–5, Jun. 2016. DOI: 10.1109/TASC.2016.2526605.

[16] A. Ballarino, "Current leads, links and buses," *Proc. of the CAS-CERN Accelerator School: Superconductivity for Accelerators (Erice, Italy)*, p. 12, 2013. DOI: 10.5170/CERN-2014-005.547.

[17] Z. Bai, G. Yan, C. Wu, *et al.*, "A novel high temperature superconducting magnetic flux pump for MRI magnets," *Cryogenics*, vol. 50, no. 10, pp. 688–692, Oct. 1, 2010. DOI: 10.1016/j.cryogenics.2010.06.021.

[18] C. Hoffmann, D. Pooke, and A. D. Caplin, "Flux pump for HTS magnets," *IEEE Transactions on Applied Superconductivity*, vol. 21, no. 3, pp. 1628–1631, Jun. 2011. DOI: 10.1109/TASC.2010.2093115.

[19] C. W. Bumby, Z. Jiang, J. G. Storey, *et al.*, "Anomalous open-circuit voltage from a high-Tc superconducting dynamo," *Applied Physics Letters*, vol. 108, no. 12, p. 122 601, Mar. 21, 2016. DOI: 10.1063/1.4943663.

[20] R. Mataira, M. Ainslie, A. Pantoja, *et al.*, "Mechanism of the high-Tc superconducting dynamo: Models and experiment," *Physical Review Applied*, vol. 14, no. 2, p. 024 012, Aug. 6, 2020. DOI: 10.1103/PhysRevApplied.14.024012.

[21] H. Ye, W. Wang, Y. Zhang, *et al.*, "A linear-motor type HTS flux pump with pumped current exceeding 640 a," *IEEE Transactions on Applied Superconductivity*, vol. 31, no. 8, pp. 1–5, Nov. 2021. DOI: 10.1109/TASC.2021.3101743.

[22] J. Geng and T. A. Coombs, "Mechanism of a high-Tc superconducting flux pump: Using alternating magnetic field to trigger flux flow," *Applied Physics Letters*, vol. 107, no. 14, p. 142 601, Oct. 5, 2015. DOI: 10.1063/1.4932950.

[23] J. Geng and T. A. Coombs, "An HTS flux pump operated by directly driving a superconductor into flux flow region in the E-J curve," *Superconductor Science and Technology*, vol. 29, no. 9, p. 095 004, Sep. 1, 2016. DOI: 10.1088/0953-2048/29/9/095004.

[24] J. D. D. Gawith, J. Geng, C. Li, *et al.*, "A half-bridge HTS transformer-rectifier flux pump with two AC field-controlled switches," *Superconductor Science and Technology*, vol. 31, no. 8, p. 085 002, Jun. 2018. DOI: 10.1088/1361-6668/aac86d.

[25] J. Ma, J. Geng, and T. A. Coombs, "Flux pumping for non-insulated and metal-insulated HTS coils," *Superconductor Science and Technology*, vol. 31, no. 1,

p. 015 018, Jan. 1, 2018. DOI: 10.1088/1361-6668/aa99f2.

[26] P. Zhou, G. Ma, Y. Deng, *et al.*, "A contactless self-regulating HTS flux pump," *IEEE Transactions on Applied Superconductivity*, vol. 30, no. 4, pp. 1–6, Jun. 2020. DOI: 10.1109/TASC.2020.2978787.

[27] Y. Zhai, P. Zhou, J. Li, *et al.*, "Performance investigation of contactless self-regulating HTS flux pump," *IEEE Transactions on Applied Superconductivity*, vol. 31, no. 5, pp. 1–5, Aug. 2021. DOI: 10.1109/TASC.2021.3073531.

[28] B. Leuw, J. Geng, J. H. P. Rice, *et al.*, "Demonstration of a half-wave superconducting transformer-rectifier flux pump (strfp) using jc(b) switches," submitted manuscript, 2021.

[29] E. H. Brandt, "Superconductors of finite thickness in a perpendicular magnetic field: Strips and slabs," *Physical Review B*, vol. 54, no. 6, pp. 4246–4264, Aug. 1, 1996. DOI: 10.1103/PhysRevB.54.4246.

[30] Y. Deng, J. Li, P. Zhou, *et al.*, "Performance optimization and verification of the transformer-rectifier flux pump for HTS magnet charging," *IEEE Transactions on Applied Superconductivity*, vol. 30, no. 4, pp. 1–5, Jun. 2020. DOI: 10.1109/TASC.2020.2990203.

[31] C. Li, J. Geng, J. Gawith, *et al.*, "Design for a persistent current switch controlled by alternating current magnetic field," *IEEE Transactions on Applied Superconductivity*, vol. 28, no. 4, pp. 1–5, Jun. 2018. DOI: 10.1109/TASC.2018.2809545.

[32] E. Mezzetti, R. Gerbaldo, G. Ghigo, *et al.*, "Control of the critical current density in YBa_2Cu3O_7-d films by means of intergrain and intragrain correlated defects," *Physical Review B*, vol. 60, no. 10, pp. 7623–7630, Sep. 1, 1999. DOI: 10.1103/PhysRevB.60.7623.

[33] N. M. Strickland, C. Hoffmann, and S. C. Wimbush, "A 1 kA-class cryogen-free critical current characterization system for superconducting coated conductors," *Review of Scientific Instruments*, vol. 85, no. 11, p. 113 907, Nov. 2014. DOI: 10.1063/1.4902139.

[34] S. C. Wimbush and N. M. Strickland, "A public database of high-temperature superconductor critical current data," *IEEE Transactions on Applied Superconductivity*, vol. 27, no. 4, pp. 1–5, Jun. 2017. DOI: 10.1109/TASC.2016.2628700.

[35] Z. Jiang, R. Toyomoto, N. Amemiya, *et al.*, "Dynamic resistance of a high- tc coated conductor wire in a perpendicular magnetic field at 77 k," *Superconductor Science and Technology*, vol. 30, no. 3, 03LT01, Mar. 1, 2017. DOI: 10.1088/1361-6668/aa54e5.

[36] COMSOL, Inc., Burlington, MA, USA, COMSOL ver 5.6,

[37] T. Benkel, M. Lao, Y. Liu, *et al.*, "T-a-formulation to model electrical machines with HTS coated conductor coils," *IEEE Transactions on Applied Superconductivity*, vol. 30, no. 6, pp. 1–7, Sep. 2020. DOI: 10.1109/TASC.2020.2968950.

[38] R. Brambilla, F. Grilli, L. Martini, *et al.*, "A finite-element method framework for modeling rotating machines with superconducting windings," *IEEE Transactions on Applied Superconductivity*, vol. 28, no. 5, pp. 1–11, Aug. 2018. DOI: 10.1109/TASC.2018.2812884.

[39] J. Geng and T. A. Coombs, "Modeling methodology for a HTS flux pump using a 2d h-formulation," *Superconductor Science and Technology*, vol. 31, no. 12, p. 125 015, Dec. 1, 2018. DOI: 10.1088/1361-6668/aae4bc.